International Journal of Pharmaceutics 576 (2020) 118978

Contents lists available at ScienceDirect

International Journal of Pharmaceutics

journal homepage: www.elsevier.com/locate/ijpharm

Continuous synthesis of drug nanocrystals by solid hollow fiber cooling crystallization

Qiuhong Liu[a,1], Xuan Zhu[a,1], Bing Wang[b], Xinyi Zhou[a], Chen Liu[a], Xuemin Gao[a], Kamalesh K. Sirkar[c,*], Dengyue Chen[a,*]

[a] School of Pharmaceutical Sciences, Xiamen University, Xiamen, Fujian 361102, China
[b] Key Laboratory of Urban Pollutant Conversion, Institute of Urban Environment, Chinese Academy of Sciences, Xiamen, Fujian 361021, China
[c] New Jersey Institute of Technology, Otto York Department of Chemical, Biological and Pharmaceutical Engineering, Newark, NJ, USA

ARTICLE INFO

Keywords:
Griseofulvin
Drug nanoparticles
Solid hollow fibers cooling crystallization
Precipitation

ABSTRACT

Size reduction of drug with poor water solubility to nanoscale is an effective way to help improve the efficacy of drug delivery to the human body. A solid hollow fiber cooling crystallization technique has been adopted to continuously produce griseofulvin drug nanoparticles under modest conditions with accurate controllability. In the solid hollow fiber cooling crystallization device, drug solution flowed through the bores of solid hollow fibers while the cooling liquid was circulated counter-currently in the shell side of the device to cool down the drug solution in the tube side. Due to intense heat exchange between the cooling liquid and the drug solution through the thin fiber walls, the temperature of drug solution decreased rapidly so that drug nanoparticles were precipitated out from the solution by sudden reduction of solubility. Through variation of the experimental conditions and parameters, the mean size of the produced nanoparticles was regulated and controlled. The nanoparticles were dispersed uniformly, the chemical structure and bonds of prepared nanoparticles was the same with as-received griseofulvin. Both raw material and NPs the polymorph(s) present form I, the melting point was 220 °C. Drug dissolution testing was also executed to verify that nanocrystals have a higher dissolution profile.

1. Introduction

Nanoparticles are of great interests in many fields including theoretical magnetics (Sun et al., 2010), cancer drug resistance (Markman et al., 2013), solar cells (Law et al., 2005), optical sensors (Pouzesh et al., 2019), drug delivery systems (Allen et al., 2013), biological systems (Albanese et al., 2012), and antimicrobial activity (Ahmed et al., 2016). Drug nanoparticles are frequently used in drug delivery systems due to their distinct properties such as large surface area, high solubility, excellent carrying capacity, controlled release, targeting to a special type of cell, and multimodality for diagnostics (Chen et al., 2016). Each drug has a therapeutic window for the best use of the drug; however, in some cases, poor water solubility of drugs limits the concentration of drugs to the target areas. Due to the unique properties of nanoparticles, reduction particle size of drug is one of the most promising way to improve the efficacy of drug delivery (Chen et al., 2011).

Currently, both top-down and bottom-up methods are used to produce drug nanoparticles (Biswas et al., 2012). Conventional top-down methods include high-pressure homogenization (HPH), stirred bead milling (SBM), chemical vapor etching technology, etc. To improve bioavailability of drugs, the HPH and SBM methods are utilized to produce uniform nanoparticles using different mechanical strategies: HPH approach mainly depends on cavitation effect to produce nanoparticles while SBM is brought upon by collisions between milling media and the solid API particles (Nakach et al., 2018). Duan reported that chemical vapor etching is used to synthesize nanoparticles with corrugated-shaped structure (Duan et al., 2018); the corrugated structure of the nanoparticles showed remarkable stability. Due to high-energy consumption, high mass loss and cost incurred, the top-down methods are gradually trending down.

Bottom-up methods generate nanoparticles popularly by precipitation and evaporation methods (Ariga et al., 2007). Dai introduced a facile method by using $SiCl_4$ as a self-assembled template to synthesize nano-sized porous silica without etching (Dai et al., 2014). Compared to conventional methods, this approach costs less and improves the performance of silica via high porosity and large surface area. Spray freeze-drying (SFD) and supercritical fluid (SCF) approaches are used widely to synthesis hydrogels (Ali et al., 2009). Using SFD method, the

* Corresponding authors.
E-mail addresses: sirkar@njit.edu (K.K. Sirkar), dchen@xmu.edu.cn (D. Chen).
[1] Q. Liu and Dr. X. Zhu contributed equally to this work and should be considered as co-first authors.

https://doi.org/10.1016/j.ijpharm.2019.118978
Received 21 June 2019; Received in revised form 11 December 2019; Accepted 16 December 2019
Available online 20 December 2019
0378-5173/

hydrogels with the large pores tend to form micrometer scale due to nucleation and growth of solvent crystals. To reduce the size of aerogel pore size to nanoscale, Clare froze the sample immediately into small-size particles and then sublimate it under low pressure to produce nano-sized hydrogels (Jiménez-Saelices et al., 2017). On the contrary, SCF technology is beneficial in that a porous structure is better produced and could conserve the nanoscale product. Supercritical fluids can replace organic solvents for their unique properties, such as no toxicity, low viscosity, reaction under medium temperature and without drying process, etc. Supercritical fluids have become a popular method to produce nanoparticles in which supercritical carbon dioxide (SCO_2) is widely used as a solvent of hydrophobic drugs (Tsang et al., 2018); this method is environmentally beneficial to produce nanoparticles without any residual solvent. To achieve quicker dissolution, the supercritical anti-solvent (SAS) process is applied to enhance the solubility of nanoscale drugs (Park et al., 2014).

However, these technologies for nanoparticle synthesis have shortcomings, such as requirement of large equipment and high pressure. Atomic layer deposition (ALD) is a useful approach to fabricate nanoparticles, whereas the process is slow and requires expensive vacuum equipment. Sol gel nanofabrication is applied to synthesize various materials and cost less, but the reaction is difficult to control. Chemical vapor deposition may produce toxic gases during the synthesis process (Biswas et al., 2012). The layer-by-layer assembly method is facile and affordable, however, the qualities and thicknesses of LBL film depend largely on experimental conditions such as pH (Ariga et al., 2007). Machmudah et al. (Machmudah et al., 2016) introduced batch and flow methods to produce porous zirconia nanoparticles with a SUS tube under a high pressure of 30 MPa. Batch reactor is also a good way to remove the phenolic compounds by stainless steel metal tube though cooling crystallization (Kontos et al., 2014). However, the tubes made of stainless steel are easily corroded without proper coatings (Wang et al., 2017).

Zarkadas and Sirkar (Zarkadas et al., 2004a; Zarkadas et al., 2004b) have already demonstrated by solving the governing heat transfer equations that the temperature differences between the hollow fiber wall and the crystallizing solution is as low as 1–2 °C due among others to the very small radial dimensions of the hollow fibers; the corresponding differences in SUS tubes are around 5–10 °C. As a result, one can have uncontrolled nucleation at different radial locations along the much larger SUS tube radius leading to a very broad crystal size distribution. Zarkadas and Sirkar (Zarkadas et al., 2004a) have carried out already a comparison between a MSMPR crystallizer and a SHFCC device. Although it would be useful to carry out a SUS tube-based crystallization, it is clear that it will have a much broader CSD than that in a SHFCC.

To avoid these problems, the solid hollow fiber cooling crystallization (SHFCC) technology (Zarkadas et al., 2004a) is adopted here to fabricate drug nanocrystals in a continuous operated manner with more accurate controllability over the product, and increased economic efficiency. In the SHFCC device, a solution of the drug to be crystallized flows evenly in the bore of many identical microns-sized solid hollow fine fibers that could provide accurately controlled micro-environment for crystallization of nanoparticles; a cold liquid flows on the shell side of this hollow fine fiber in a countercurrent direction setting up a rapid and highly efficient heat exchange, thus very high supersaturation is created instantaneously leading to rapid crystallization of the drug inside the entire hollow fibers (Zarkadas et al., 2004a). Compared to metallic materials, polymeric materials can be much more resistant to corrosion and dirt accumulation. Polymeric hollow fiber heat exchangers can have thermal conductance/volume 3–10 times larger than shell-and-tube heat exchangers (Zarkadas et al., 2004b). Solid hollow fiber cooling crystallization devices utilize such solid polymeric hollow fibers for heat exchange. In the SHFCC device, the drug solution flows through the bore of solid hollow fibers, while cooling liquid is circulated counter-currently in the shell side of the solid hollow fibers. Owing to the temperature differential, the drug particles crystallized/precipitated from feed solution to be collected. Zarkadas used water-soluble paracetamol as a drug model and found that the mean size of crystals was impacted by temperature variation of the cooling liquid (Zarkadas et al., 2007). For this, heat exchange could be used to control the size easily and had a promising application in the preparation of nanoparticles. In the previous study (Chen et al., 2016), we have used the SHFCC method to obtain micron-size drug crystals with the size around 10 μm in a continuous fashion, as well as continuous polymer coating of submicron sized silica particles (0.5 μm) by different polymers.

In this study, the SHFCC technique was further developed to produce nano-sized drug particles of griseofulvin (GF) continuously under modest conditions, and the product quality could be controlled by the variation of different parameters. This novel SHFCC device was developed to produce the drug nanoparticles in a continuous manner which was in accordance with the FDA's new policy and industry trend. By switching to continuous operation, we can produce the product in a more controllable, economical and accurate way. To have excellent heat exchange, the size of the inner diameter of solid hollow fibers, which are key to the SHFCC module, is chosen to be in the millimeter range. With the size of hollow fibers smaller, the temperature difference between the fiber centerline and the wall decreased, which generated a relatively uniform heat exchange conditions; meanwhile the wall thickness was small enough to help rapid heat transfer through the wall. The module contained a number of parallelly-placed hollow fibers inside the shell to ensure the heat transfer through each hollow fiber can be carried out simultaneously and efficiently. The scale-up was also easy to achieve just by proportionally increasing the numbers of hollow fibers in the tube side. The morphology of particles was measured by Transmission electron microscopy (TEM) and Scanning electron microscope (SEM); Raman, X-ray diffractometion (XRD) and Fourier transform infrared spectrometer (FT-IR) were used to determine the compositional properties of the particles; Synchronous TG-DSC thermal analyzer (DSC) was used to compare the thermal properties of the nanoparticles with those of the as supplied material; the dissolution rate was also investigated to compared the dissolution property between the as-received drug and produced nanocrystals of the drug.

2. Materials and methods

2.1. Materials

Griseofulvin (GF, purity 99.2%) drug in the form of particles was prepared by a batch-type reactor from Yuanchenggongchuang Technology Co. Ltd (Wuhan, China) and used without any treatment. Acetone acting as the solvent for GF was purchased from Lvyin Chemical Co. Ltd (Xiamen, China). An aqueous solution of 95% by volume of ethanol (95% ethanol) was obtained from Dahao fine Chemical Co. Ltd (Shantou, China). All materials were used as received.

2.2. Experimental method

As shown in Fig. 1 (a), the SHFCC system was made of four components: water bath section; circulating coolant section; heat exchange section and filtering section. In the water bath section (DF-101S, Hangzhou Gengyu Instrument Co. Ltd, Hangzhou, Zhejiang, China), the as-received GF powder was first dissolved in acetone at a saturation concentration (42.6 mg/mL) at a bath temperature of 40 °C with magnetic stirring. Using a peristaltic pump, the acetone solution of griseofulvin was introduced through the interior of solid hollow fibers at a flow rate of 17 mL/min (unless otherwise mentioned) at a constant temperature of 40 °C. At the same time, ethanol (95%) as cooling liquid at a temperature of −10 °C (unless otherwise mentioned) was circulated counter-currently in the shell side of the hollow fibers. Due to the quick exchange of heat between the drug solution and the cooling

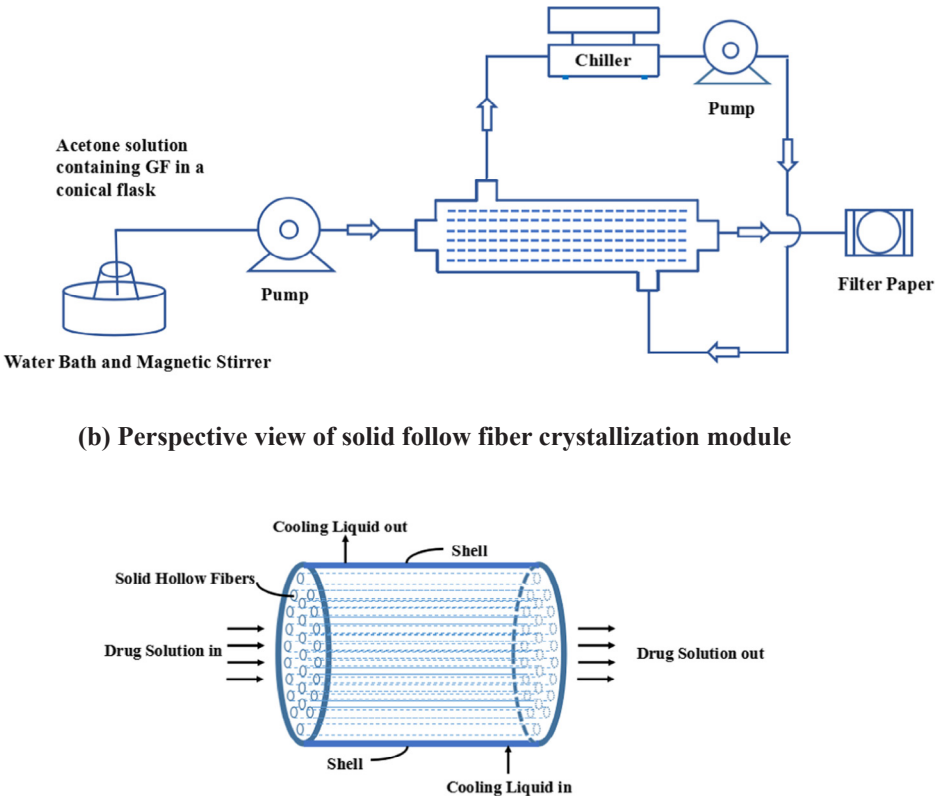

Fig. 1. (a) Flow diagram of the solid hollow fiber crystallization process; (b) Perspective view of solid hollow fiber crystallization module.

liquid through the very thin hollow fiber walls, the temperature of drug solution decreased rapidly leading to the precipitation of GF nanoparticles. A filter system was placed underneath the device outlet to collect the drug nanoparticles. The particles were freeze-dried and stored under the temperature of −20 °C.

A perspective view of solid hollow fibers cooling crystallization (SHFCC) shown in Fig. 1 (b) exhibited the principle of liquid flow and heat exchange. As a kernel of heat exchange section in SHFCC system, the SHFCC module contained 40 solid hollow fibers inside the tube; these fibers were made of polyetherimide (Sabic PEI Ultem1000) with an outer diameter (O.D) of 700 μm and an inner diameter (I.D) of 500 μm. These hollow fibers with an effective length of 32 cm were placed inside a tubular shell, which had an O.D of 1.8 cm.

2.3. Particle characterization

2.3.1. TEM

The GF particle size and morphology were investigated by a transmission electron microscopy (Tecnai G, Spirit, FEI, Hong Kong). For characterization, the samples were first dispersed homogeneously in water by using an ultrasonic bath; then a droplet was placed on a carbon coated TEM grid to allow the evaporation of the solvent.

2.3.2. SEM

Microstructures of samples were investigated with scanning electron microscope (Supra 55, Zeiss, Oberkochen, Germany). The prepared particles were dissolved in water, and a drop of suspension was put on a silica slice and dried in an oven. The samples were observed after spraying gold in a high vacuum environment for 30 s.

2.3.3. DLS

Dynamic light scattering (DLS) analyzer (Nano-ZS, Malvern Instruments Ltd, UK) was applied to obtain the mean size and distribution of the particles. The Brownian motion of particles in dispersion produced the fluctuation of scattered light and then the equipment detected the scattered light. For the detection of particle size distribution, the sample was dispersed in water at a concentration of 0.5 mg/mL.

2.3.4. XRD

The structural properties of the samples were measured by Ultima IV X-ray diffractometer (XRD, Rigaku, Matsubara-cho, Japan) and the wavelength of Cu-Kα radiation was 0.15418 nm, operating at 40 kV and 30 mA in 2θ range of 0–40°. The scanning rate was set at 15°/ min with a step size of 0.02°.

2.3.5. DSC

The thermal analysis of GF particles was investigated with a Synchronous TG-DSC thermal analyzer (STA 449 F5 Jupiter, Netzsch, Bavaria, Germany). A sample of 5 mg was placed in a hermetically sealed alumina crucible, in a temperature range of 75 °C to 250 °C with a ramp of 10 °C/ min. Nitrogen flow rate was set at 20 mL/min.

2.3.6. FT-IR

A Fourier transform infrared spectrometer (Bruker, Germany) was performed to detect whether the chemical groups of samples altered. A mixture of drug particles and potassium bromide was pulverized by an agate mortar and dried in an oven before the FT-IR spectra were taken in the spectral range from 400 to 4000 cm^{-1}.

2.3.7. In vitro dissolution testing

For comparing the dissolution performance between the as-received GF particles and the produced nanoparticles, a dissolution tester (ZRS-8GD, Tianjin Tianda Tianfa, Tianjin, China) was operated using the paddle method to determine the cumulative dissolution of the samples. With the equipment operated at a rate of 100 rpm under a temperature

of 37 °C, each sample weighing 15 mg precisely was added to 500 mL phosphate buffer saline (PBS) with pH of 6.8 in a dissolution cup (maximum volume of 1 L). At time intervals of 5, 10, 15, 20, 25, 30, 40, 50, 60, 70, 80, 90, 110, 130, 150, 180, 210 min, 5 mL solution (containing the dissolving sample) was taken out respectively from the cup and the same amount of fresh PBS was added in. Getting through a filter with pore diameter of 0.45 μm, the optical density value of solution was detected by an ultraviolet spectrophotometer (UV-1750, Shimadzu, Japan) at a wavelength of 292 nm. Compared to a standard curve, the concentrations at all times were obtained to determine the dissolution performance of as-received GF and nanoparticles. The dissolution difference between as-received GF and drug nanocrystals was determined via similarity factor (f_2).

3. Results and discussion

3.1. Characterization of GF nanocrystals

3.1.1. Characterization of morphology and size

Under a flow rate of 17 mL/min and T-differential of 50 °C, the size of particle was determined to be around 200 nm. The optimization experiments were performed and the yield was about 12.4% while 60% GF remained in solution. As shown in Fig. 2, the mean particle size of produced nanoparticles and as-received drug powder were obtained by dynamic light scattering (DLS) to be 189.8 ± 7.5 nm and 4056 ± 100.5 nm, respectively. The much smaller size of the produced drug nanoparticles could be attributed to the following reasons: the very large surface area/volume ratio for the solid hollow fiber membranes could increase the heat transfer efficiency between the cooling liquid and the drug solution that lead to a rapid precipitation of the drug nanocrystals; then the small-sized hollow fiber interiors could help regulate the size of produced nanocrystals before being pumping out to the outlet. The produced nanocrystals were stored up to 30 days after the collection, and the particle size of product remain relatively stable after proper storage as shown in Fig. 3. It is suggested that the thin hollow fiber walls and their small diameter in the SHFCC device could accurately control the temperature profile and reduce its variation across the radial dimension so that the synthesized particle size could be controlled through the adjustment of operating conditions.

TEM images shown in Fig. 4(a) and Fig. 4(b) illustrate the appearances of prepared nanoparticles and as-received GF. With twentyfold difference in size, the particle size of drug powder and prepared nanoparticles (about 200 nm) were in accordance with the result shown in DLS. The as-received GF showed agglomeration and irregular shape while the produced drug nanoparticles were dispersed uniformly in the picture. SEM was further used to measure the morphology and structure of as-received GF and drug nanoparticles. As shown in Fig. 5(a), the size of as-received GF was about 4 μm with very thick agglomeration and rough surface at the magnification scale of 10.00 KX, while the

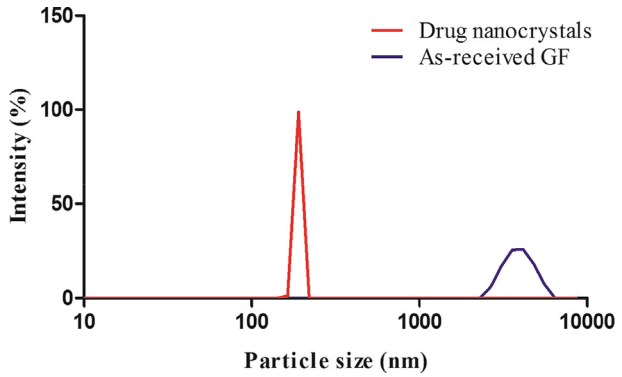

Fig. 2. The DLS-based size distribution of nanocrystals and as-received GF without any treatment.

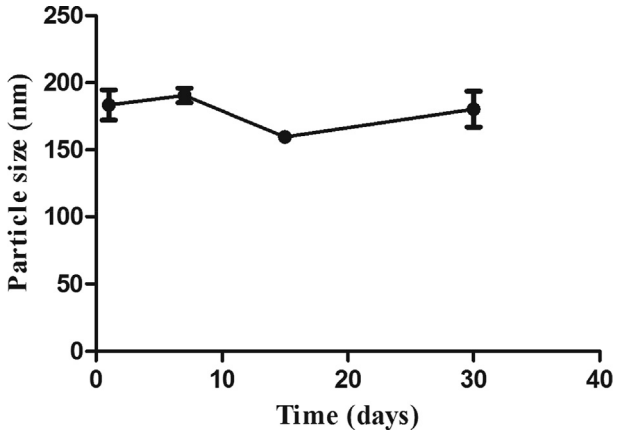

Fig. 3. The stability test of prepared nanoparticles *(mean ± SD, n = 3)*.

produced nanoparticles had a particle size around 200 nm with a smooth crystal structure in Fig. 5(b). Besides, Fig. 5(c) indicated an excellent dispersity for the drug nanocrystals which further suggested successful production of fine nanocrystals by the SHFCC device.

3.1.2. Chemical structure analysis

FT-IR result shown in Fig. 6 was used to analyze the chemical structure and bonds of prepared nanoparticles and the as-received GF. The results showed that the characteristic peaks at 1460 cm^{-1}, 1504 cm^{-1}, 1802 cm^{-1} and 1615 cm^{-1} were derived from the skeleton vibration (v C=C) of the benzene ring and the presence of peak at 2988 cm^{-1} was C–H stretching vibration (v C–H). Simultaneously, the presence of peaks at 1659 cm^{-1} and 1710 cm^{-1} were derived from the characteristic peak of C=O stretching vibration (v C=O). Compared to as-received GF, the chemical bonds of prepared nanoparticles by SHFCC device did not make any difference which further suggests that the synthesized GF nanoparticles retain the same structure as that of the original drug.

3.1.3. Crystallinity analysis

Results of XRD analysis of prepared nanoparticles and the as-received GF shown in Fig. 7 confirmed the crystallinity of nanoparticles. The polymorph of original griseofulvin was form I (De Gioannis et al., 2004a; De Gioannis et al., 2004b; Su et al., 2018; Mahieu et al., 2013). Compared with as-received GF, the location of the peaks in the case of nanoparticles coincided with those of as-received GF indicating that there was no crystal form transformation. The polymorph was form I for both prepared nanoparticles and the as-received GF, suggesting that the SHFCC process did not alter the crystallinity of the GF drug particles.

Melting temperatures of different griseofulvin polymorphs were discriminatory, and the temperature of form I was 220 ± 1 °C, form II was 214 ± 1 °C, form III was 205 ± 1 °C (Mahieu et al., 2013). Thermal analyses for prepared nanoparticles and as-received GF detected with TG-DSC thermal analyzer determined that the structure of drug nanocrystals did not change when processed with the SHFCC device. According to testing results shown in Fig. 8, the DSC curves nearly overlap except that the melting points had a slight difference for prepared nanoparticles and as-received GF. No significant difference in melting point indicated crystalline nature of nanoparticles was the same as that of the as-received GF. However, the peak area of nanoparticles (about 94.01 J/g) was larger than drug powder (peak area about 71.47 J/g) demonstrating that the prepared nanoparticles had higher crystallinity, which was in agreement with the XRD result. No obvious loss of mass or melting points change for prepared nanoparticles were observed during synchronous TG-DSC thermal analysis.

3.1.4. Dissolution testing

The dissolution and release of drug directly affect the absorption of

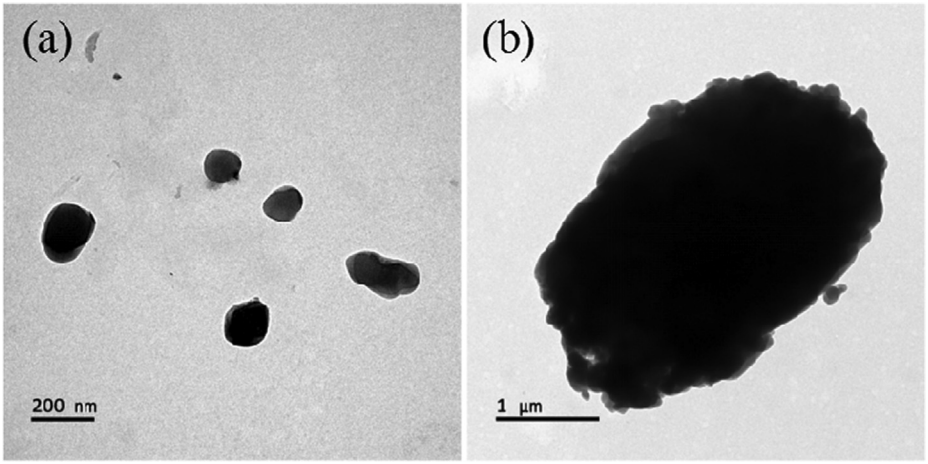

Fig. 4. TEM micrographs of (a) nanoparticles fabricated by SHFCC device and (b) as-received GF without any treatment.

drug in human body; therefore, dissolution is closely related to the efficacy of drugs. Compared to the size of as-received GF, nanoscale particles had a higher specific surface area for their small dimension, and large contact area further promotes drug dissolution and absorption as exhibited in Fig. 9 indicating that the drug nanocrystals had a higher dissolution profile than that of the as-received GF (the experiment was repeated three times). The cumulative dissolution of prepared nanoparticles reached up to 20% at 5 min whereas the as-received GF crystals required about 40 min to reach a cumulative dissolution of 20%. Thus, the dissolution rates at the beginning were higher than those of as-received micron-scale drug crystals produced by conventional batch reactor for almost an order of magnitude. After as-received powder dissolution for 180 min and 210 min, the cumulative release of powder was up to 54.2% and 54.6% in succession; meanwhile, over 60% prepared nanoparticles dissolved in PBS at 110 min and did not increase remarkably. A statistical analysis was used to determine the dissolution difference between as-received GF and drug nanocrystals. The similarity factor f_2 can be calculated as

$$f_2 = 50 \cdot \log\left\{1 + \left(\frac{1}{n}\right)\sum_{t=1}^{n}[(R_t - T_t)^2]^{-0.5} \cdot 100\right\} \quad (1)$$

where n was number of time points; R_t was dissolution value of the as-received GF at time t; T_t was dissolution value of the drug nanocrystals at time t. The prepared nanoparticles did not exhibit similar drug release profile compared to that of as-received powder with f_2 value of 30.1 which identified there existed statistical significance ($p < 0.05$) in the drug release.

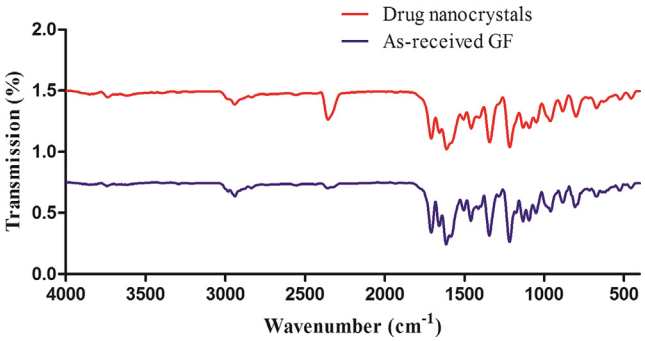

Fig. 6. FT-IR images of prepared nanoparticles and as-received GF without any treatment.

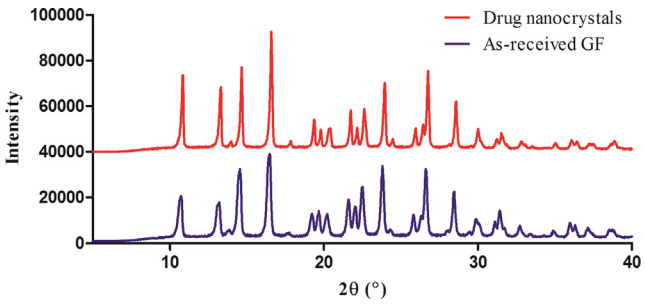

Fig. 7. XRD patterns of prepared drug nanocrystals and as-received GF without any treatment.

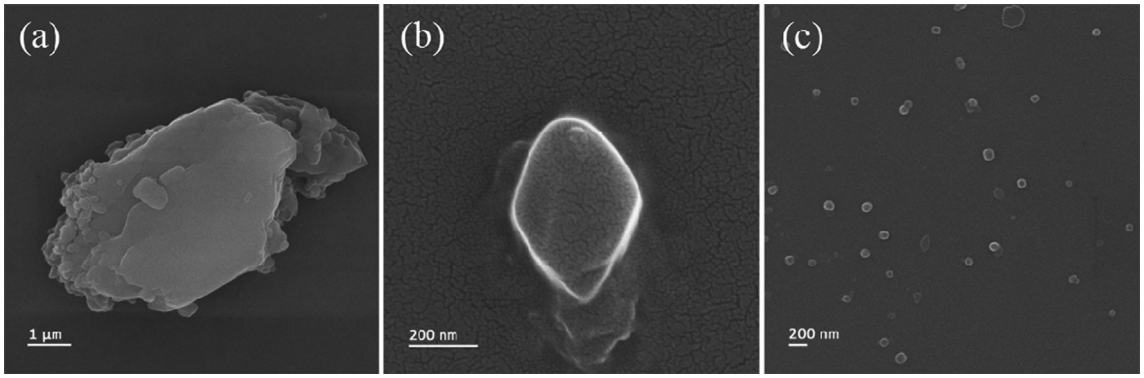

Fig. 5. SEM micrographs: (a) as-received GF without any treatment at a magnification of 10.00 KX; (b) prepared GF nanoparticles at a magnification of 20.00 KX; (c) prepared GF nanoparticles at a magnification of 80.00 KX.

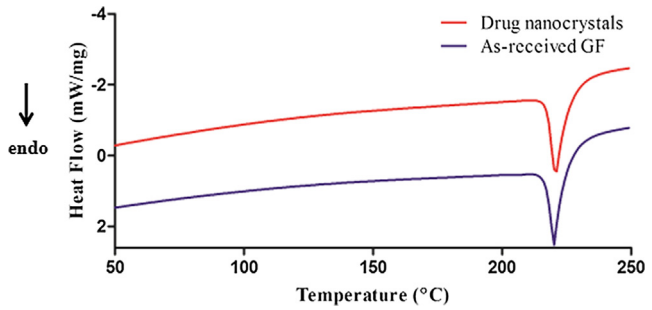

Fig. 8. DSC results of prepared drug nanocrystals and as-received GF without any treatment.

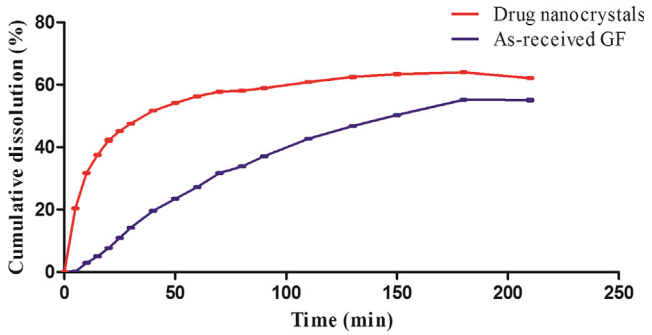

Fig. 9. Cumulative dissolution results of prepared nanocrystals and as-received GF particles without any treatment *(mean ± SD, n = 3)*.

3.2. The variation of flow rate for drug solution

The flow rate of the drug solution could impact the particle size of the drug nanocrystals through the change of the residence time for different flow rates as well as the mixing conditions. Faster flow rate could reduce the residence time of the crystallization process to decrease the particle size. In addition, the mixing condition could be also intensified due to the high feed side flow velocity inside of the hollow fibers. Therefore, a series of flow rates (8.5, 17 and 25.5 mL/min) were utilized as shown in Table 1. Except for flow rate, other factors in experiment remained constant: saturation concentration at 42.56 mg/mL; the temperature of water bath was setting at 40 °C; the temperature of cooling liquid was set at −15 °C; SHFCC device without any change and so on.

As shown in Fig. 10, the mean size of the synthesized GF nanocrystals was 407.2 nm, 276.2 nm and 172.6 nm, respectively under condition A1, A2 and A3. The results were generally in accordance with the TEM pictures of Fig. 11. With an increase in the flow rate of the drug solution, the mean size of nanoparticles decreased gradually on account of shorter residence time in the hollow fibers. Keeping other factors constant, the increased flow rate of drug solution led to a shortened duration of heat exchange, and further impeded the growth of crystals. Meanwhile at a large flow rate of 25.5 mL/min (condition A3), very low mass of nanoparticles precipitated on a filter paper since there was not enough time to grow crystals. Compared to the mean size and morphology of nanoparticles under different flow rate, the particle surface had no significant change. By simply changing the flow rate of drug of solution, the yield of nanocrystals increased.

3.3. The variation of cooling temperature of circulating liquid

Cooling temperature of the shell side fluid plays an important part in the crystallization process since it directly affects the supersaturation level of the drug solution and the nucleation rate in the lumen side. In order to study the heat exchange impact due to the change of cooling temperature, the temperature of cooling liquid was set at 0, −5, −10

Table 1
Particle size of the produced drug nanocrystals under the variation of flow rate of drug solution (n = 3).

Experimental	Temperature of water bath (°C)	Temperature of cooling liquid (°C)	ΔT (°C)	Flow rate of drug solution (mL/min)	Residence time (s)	Mean (nm)	Standard Deviation (nm)	D_{10} (nm)	D_{50} (nm)	d_{90} (nm)	Yield (%)
A1	40	−15	55	8.5	17.7	407.2	26.1	299	414	523	13.4
A2	40	−15	55	17	8.9	276.2	11.8	250	286	331	10.2
A3	40	−15	55	25.5	5.9	172.6	7.8	143	164	188	3.6

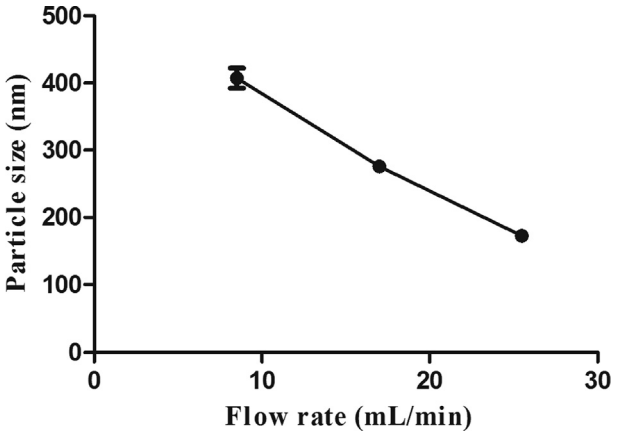

Fig. 10. Particle size under variation of flow rate and temperature differential of 55 °C *(mean ± SD, n = 3)*.

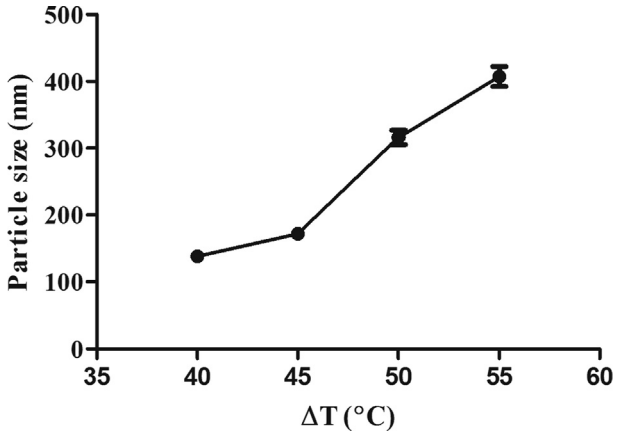

Fig. 12. Variation of particle size of produced GF drug nanocrystals with temperature differential *(mean ± SD, n = 3)*.

and −15 °C respectively (namely B1, B2, B3 and B4) in the experiments. Other parameters in experiment remained identical for these four experimental groups: a saturation concentration at 42.56 mg/mL, the water bath temperature at 40 °C, and the drug solution flow rate at 8.5 mL/min.

Due to the cooling temperature decrease, the temperature differential increased. As shown in Fig. 12, temperature differential increased led to an increase in the mean size of nanoparticles. Under conditions B1, B2, B3 and B4, the mean size of nanoparticles was respectively at 138.3 nm, 172.1 nm, 316.0 nm and 407.2 nm as shown in Table 2. At low supersaturation, crystals can grow faster than they nucleate resulting in a larger crystal size distribution. However, at higher supersaturation, crystal nucleation dominated crystal growth, ultimately resulting in smaller crystals. In our experiment, since the drug griseofulvin was not that sensitive to the temperature reduction, it produced relatively low supersaturation that led to the larger crystal size. Moreover, during the initial stage of reaction, it did produce more nuclei due to larger ΔT induced supersaturation. It was easier for these many nuclei to agglomerate and grow in the module due to the nature of continuous liquid flow movement that swept together some of the drug particles. So larger ΔT could essentially promote the generation and growth of the nanocrystals under same residence time resulting in the increase of the particle size and yield.

4. Conclusions

A solid hollow fiber cooling crystallization (SHFCC) technology was developed to continuously fabricate drug nanocrystals under modest conditions. A compact module could not only be operated in a continuous production mode to feed the modern pharmaceutical industry needs, but also be easily scaled up due to the unique interior design as proved by the control group. The accurate control of the precipitation temperature helped precisely adjust the particle size and dispersity of the produced drug nanocrystals. Besides, it was found that the drug solution flow rate and the cooling temperature were two critical parameters that could largely impact the quality and size of the produced GF nanocrystals.

Increasing the flow rate of the drug solution from 8.5 mL/min to 25.5 mL/min led to the shortening of the residence time, and further impeded the nucleation and the growth of drug nanocrystals. With enlarging temperature differential between the inlet and outlet, the mean size of nanoparticles increased, however, most of qualities of nanoparticles remained identical and stable which further suggested that this cooling crystallization method would not alter the quality of the original drug.

The SHFCC technology is suggested as suitable for continuous nanoparticle synthesis with relatively low-energy cost and easy operation including possible large-scale production. The prepared uniform and free-flowing drug nanocrystals further demonstrate that the SHFCC method had a promising application in industrial production of drug nanoparticles under continuous and controllable condition.

CRediT authorship contribution statement

Qiuhong Liu: Writing - original draft. **Xuan Zhu:** Investigation, Methodology. **Bing Wang:** Project administration. **Xinyi Zhou:** Formal analysis. **Chen Liu:** Validation. **Xuemin Gao:** Resources. **Kamalesh K. Sirkar:** Conceptualization. **Dengyue Chen:** Funding acquisition, Writing - review & editing, Supervision.

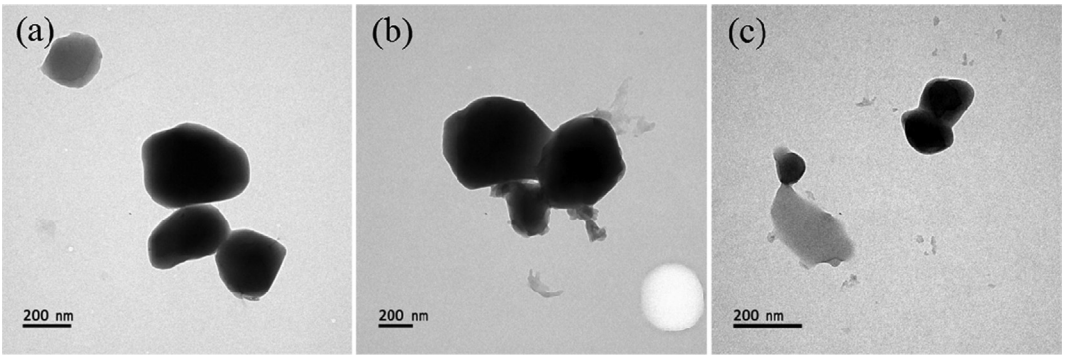

Fig. 11. TEM images of prepared nanoparticles under conditions of (a) A1, (b) A2, (c) A3.

Table 2
Particle size of the drug nanocrystals under variation of cooling temperature (n = 3).

Experimental	Temperature of water bath (°C)	Temperature of cooling liquid (°C)	ΔT (°C)	Flow rate for drug solution (mL/min)	Mean (nm)	Standard Deviation (nm)	d_{10} (nm)	D_{50} (nm)	d_{90} (nm)	Yield (%)
B1	40	0	40	8.5	138.3	12.7	109	124	140	7.3
B2	40	−5	45	8.5	172.1	7.3	142	163	189	8.8
B3	40	−10	50	8.5	316.0	18.5	284	329	381	10.7
B4	40	−15	55	8.5	407.2	26.1	299	414	523	13.4

Declaration of Competing Interest

The authors declare that they have no known competing financial interests or personal relationships that could have appeared to influence the work reported in this paper.

Acknowledgements

This work was supported by the National Natural Science Foundation of China [grant number 21706221, 81772278]; the Natural Science Foundation of Fujian Province [grant number 2018J05143]; the Fundamental Research Funds for the Central Universities [grant number 20720190077] and Educational and Scientific Foundation of Fujian Province for Young and Middle-aged Teachers [grant number JAT170009].

Appendix A. Supplementary material

Supplementary data to this article can be found online at https://doi.org/10.1016/j.ijpharm.2019.118978.

References

Sun, S., Murray, C.B., Weller, D., Folks, L., Moser, A., 2010. Monodisperse FePt nanoparticles and ferromagnetic FePt nanocrystal superlattices. Science 287, 1989–1992.
Markman, J.L., Rekechenetskiy, A., Holler, E., Ljubimova, J.Y., 2013. Nanomedicine therapeutic approaches to overcome cancer drug resistance. Adv. Drug Deliv. Rev. 65, 1866–1879.
Law, M., Greene, L.E., Johnson, J.C., Saykally, R., Yang, P., 2005. Nanowire dye-sensitized solar cells. Nat. Mater. 4, 455–459.
Pouzesh, M., Nekouei, S., Ali, M., Zadeh, F., 2019. Fabrication of stable copper nanoparticles embedded in nanocellulose film as a bionanocomposite plasmonic sensor and thereof for optical sensing of cyanide ion in water samples. Cellulose 26, 4945–4956.
Allen, T.M., Cullis, P.R., 2013. Liposomal drug delivery systems: From concept to clinical applications. Adv. Drug Deliv. Rev. 65, 36–48.
Albanese, A., Tang, P.S., Chan, W.C.W., 2012. The effect of nanoparticle size, shape, and surface chemistry on biological systems. Annu. Rev. Biomed. Eng. 14, 1–16.
Ahmed, S., Ahmad, M., Swami, B.L., Ikram, S., 2016. A review on plants extract mediated synthesis of silver nanoparticles for antimicrobial applications: a green expertise. J. Adv. Res. 7, 17–28.
Chen, G., Roy, I., Yang, C., Prasad, P.N., 2016a. Nanochemistry and nanomedicine for nanoparticle-based diagnostics and therapy. Chem. Rev. 116, 2826–2885.
Chen, H., Khemtong, C., Yang, X., Chang, X., Gao, J., 2011. Nanonization strategies for poorly water-soluble drugs. Drug Discov. Today 16, 354–360.
Biswas, A., Bayer, I.S., Biris, A.S., Wang, T., Dervishi, E., Faupel, F., 2012. Advances in top-down and bottom-up surface nanofabrication: techniques, applications & future prospects. Adv. Colloid Interface Sci. 170, 2–27.
Nakach, M., Authelin, J.R., Perrin, M.A., Lakkireddy, H.R., 2018. Comparison of high pressure homogenization and stirred bead milling for the production of nano-crystalline suspensions. Int. J. Pharm. 547, 61–71.
Duan, X., Ma, C., Jin, W., Ma, X., Guo, L., Wei, S.H., Yu, J., Wu, Y., 2018. The stabilization mechanism and size effect of nonpolar-to-polar crystallography facet tailored ZnO nano/micro rods via a top-down strategy. Phys. Chem. Chem. Phys. 20, 18455–18462.
Ariga, K., Hill, J.P., Ji, Q., 2007. Layer-by-layer assembly as a versatile bottom-up nanofabrication technique for exploratory research and realistic application. Phys. Chem. Chem. Phys. 9, 2319–2340.
Dai, F., Zai, J., Yi, R., Gordin, M.L., Sohn, H., Chen, S., Wang, D., 2014. Bottom-up synthesis of high surface area mesoporous crystalline silicon and evaluation of its hydrogen evolution performance. Nat. Commun. 5, 3605.
Ali, H.S.M., York, P., Blagden, N., 2009. Preparation of hydrocortisone nanosuspension through a bottom-up nanoprecipitation technique using microfluidic reactors. Int. J. Pharm. 375, 107–113.
Jiménez-Saelices, C., Seantier, B., Cathala, B., Grohens, Y., 2017. Spray freeze-dried nanofibrillated cellulose aerogels with thermal superinsulating properties. Carbohydr. Polym. 157, 105–113.
Tsang, M.P., Philippot, G., Aymonier, C., Sonnemann, G., 2018. Supercritical fluid flow synthesis to support sustainable production of engineered nanomaterials: case study of titanium dioxide. ACS Sustain. Chem. Eng. 6, 5142–5151.
Park, J., Cho, W., Kang, H., Lee, B.B.J., Kim, T.S., Hwang, S.J., 2014. Effect of operating parameters on PVP/tadalafil solid dispersions prepared using supercritical anti-solvent process. J. Supercrit. Fluids 90, 126–133.
Machmudah, S., Prastuti, O.P., Widiyastuti, Winardi, S., Wahyudiono, Kanda, H., Goto, M., 2016. Macroporous zirconia particles prepared by subcritical water in batch and flow processes. Res. Chem. Intermed. 42, 5367–5385.
Kontos, S.S., Koutsoukos, P.G., Paraskeva, C.A., 2014. Removal and recovery of phenolic compounds from olive mill wastewater by cooling crystallization. Chem. Eng. J. 251, 319–328.
Wang, Y., Gao, F., Yang, J., Zhu, Y., Fang, C., Wang, S., Zhao, G., 2017. Comparative study on corrosion characteristics of Al_2O_3/316L and TiO_2/316L stainless steel in supercritical water. Int. J. Hydrogen Energy 42, 19836–19842.
Zarkadas, D.M., Sirkar, K.K., 2004a. Solid hollow fiber cooling crystallization. Ind. Eng. Chem. Res. 43, 7163–7180.
Zarkadas, D.M., Sirkar, K.K., 2004b. Polymeric hollow fiber heat exchangers: an alternative for lower temperature applications. Ind. Eng. Chem. Res. 43, 8093–8106.
Zarkadas, D.M., Sirkar, K.K., 2007. Cooling crystallization of paracetamol in hollow fiber devices. Ind. Eng. Chem. Res. 46, 2928–2935.
Chen, D., Singh, D., Sirkar, K.K., Pfeffer, R., 2016b. Continuous preparation of polymer coated drug crystals by solid hollow fiber membrane-based cooling crystallization. Int. J. Pharm. 499, 395–402.
De Gioannis, B., Vega Gonzalez, A., Subra, P., 2004a. Anti-solvent and co-solvent effect of CO_2 on the solubility of griseofulvin in acetone and ethanol solutions. J. Supercrit. Fluids 29, 49–57.
De Gioannis, B., Jestin, P., Subra, P., 2004b. Morphology and growth control of griseofulvin recrystallized by compressed carbon dioxide as antisolvent. J. Cryst. Growth 262, 519–526.
Su, Y., Xu, J., Shi, Q., Yu, L., Cai, T., 2018. Polymorphism of griseofulvin: Concomitant crystallization from the melt and a single crystal structure of a metastable polymorph with anomalously large thermal expansion. Chem. Commun. 54, 358–361.
Mahieu, A., Willart, J.F., Dudognon, E., Eddleston, M.D., Jones, W., Danede, F., Descamps, M., 2013. On the polymorphism of griseofulvin: Identification of two additional polymorphs. J. Pharm. Sci. 102, 462–468.